# Transfer reactions for the $^{50}$Ti + $^{90}$Zr system below the Coulomb barrier

H. J. Kim and J. Gomez del Campo
*Oak Ridge National Laboratory, Oak Ridge, Tennessee 37831*

M. M. Hindi
*Tennessee Technological University, Cookville, Tennessee 38501*

D. Shapira and P. H. Stelson
*Oak Ridge National Laboratory, Oak Ridge, Tennessee 37831*

(Received 6 July 1988)

The analysis of quasielastic cross section data for the $^{90}$Zr projectile plus $^{50}$Ti target system shows that the probability for $^{50}$Ti($^{90}$Zr, $^{49}$Ti)$^{91}$Zr, $1n$-transfer reaction near the barrier is much larger than estimates based on semiclassical theory. The probability for $^{50}$Ti($^{90}$Zr,$^{51}$V)$^{89}$Y, $1p$-transfer reaction, on the other hand, agrees with the same theory. The internuclear distance where the $1n$-transfer probability first deviates from tunneling predictions coincides with the threshold of the fusion barrier distribution deduced from the experimental fusion cross sections of the $^{50}$Ti+$^{90}$Zr system, suggesting a common mechanism for the large enhancement of $1n$-transfer and fusion cross sections.

Transfer reactions between heavy nuclei at near-barrier energies are well described by semiclassical theories in which the reactions are assumed to occur on classically prescribed orbits; examples can be found in Refs. 1 and 2 for collisions between light and medium nuclei, in Refs. 3 and 4 for medium and medium nuclei, and in Ref. 5 for very heavy nuclei. A simple and clear picture emerges from these examples: At energies below and near the barrier, nucleon-transfer reactions proceed via the tunneling of valence nucleons between the interacting nuclei on the classical orbit, but the tunneling evolves into a grazing reaction as the energy exceeds the interaction barrier.

Cross sections for a number of element ($Z$)- and mass ($M$)-identified ejectiles resulting from the $^{90}$Zr-beam bombardment of $^{50}$Ti were measured for four bombarding energies in the 274–303-MeV range and lab angles ranging from 8° to 23° with 2° and 3° steps. The traditional role of target and projectile was reversed in this study in order to measure cross sections for large c.m. angles. Target and targetlike particles ejected from thin (30 and 70 $\mu$g/cm$^2$) targets were detected by a position-sensitive gas-filled-detector system[6] placed at the focal plane of the Oak Ridge National Laboratory (ORNL) split-pole spectrometer. The $Z$ of ejectiles was identified from the energy ($E$) and energy-loss ($\Delta E$) data while the $M$ identification was made from the $E$ and magnetic rigidity ($B\rho$) data. Figure 1 illustrates typical $Z$ and $M$ resolutions. An Si(Au) detector placed at a fixed angle (42°) provided relative as well as absolute normalization factors. (Elastic scattering was assumed to be pure Rutherford at this angle.) A single peak with a low-energy tail dominates all observed target-ejectile ($^{50}$Ti) focal-plane spectra. The "elastic" peak broadens and its tail becomes more extensive with increasing angle (at given energy) and with increasing energy (at given angle), indicating the contribution to the peak from numerous but weak inelastic excitations. The resolution ($\sim$1.8 MeV) was not sufficient to resolve individual peaks. A peak (or bump) broader than the resolution dominates the transfer-ejectile ($^{49}$Ti and $^{51}$V) spectra, indicating that numerous transitions contribute to the transfer peak also. Energy-integrated differential cross sections for $^{49}$Ti, $^{50}$Ti, and $^{51}$V ejectiles were obtained from the focal-plane spectra for the dominant charge

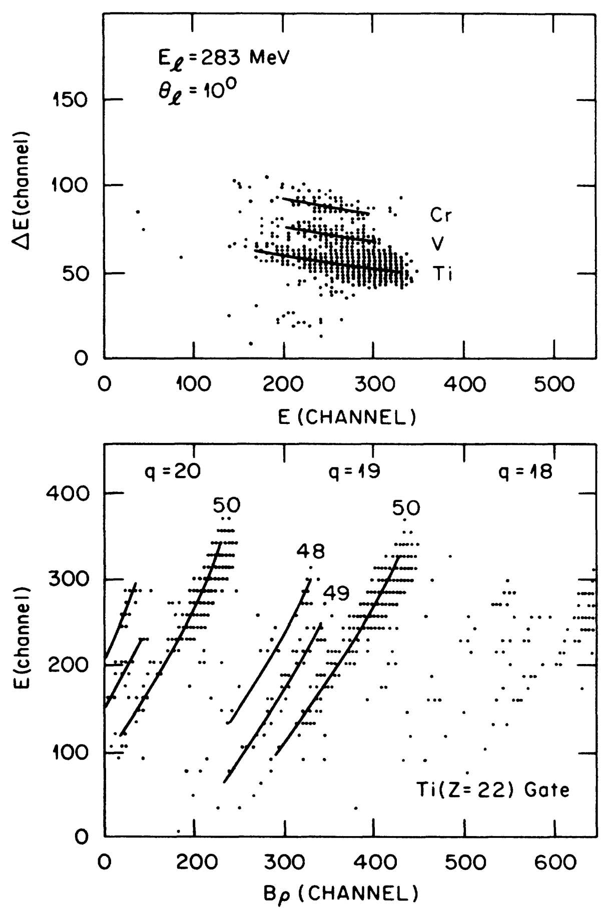


FIG. 1. A $\Delta E$ vs $E$ and a $Z$-gated $E$ vs $B\rho$ map. The curved lines show the positions of three prominent ejectile elements ($Z=22$, 23, and 24) on the $\Delta E$ vs $E$ map and of $M=^{48}$Ti, $^{49}$Ti, and $^{50}$Ti ($Z=22$) isotopes on the $q=19$–20 portion of the $Z$-gated $E$ vs $B\rho$ map.

 

TABLE I. Cross-section ratios. Statistical errors are shown in parentheses. $d\sigma_{qe}/d\sigma_{Ruth}$ values are subject to ±15% uncertainty.

| $E_{lab}$ (MeV) | $\theta_{lab}$ (deg) | $d\sigma_{qe}/d\sigma_{Ruth}$ | $d\sigma_{1n}/d\sigma_{qe}$ (%) | $d\sigma_{1P}/d\sigma_{qe}$ (%) |
|---|---|---|---|---|
| | 8 | 0.85(0.018) | 0.7(0.5) | 0.3(0.3) |
| | 10 | 0.89(0.029) | | |
| 274 | 12 | 0.92(0.019) | | |
| | 14 | 0.94(0.020) | | |
| | 23 | 1.00(0.012)[a] | | |
| | 10 | 0.81(0.018) | 1.16(0.24) | 1.04(0.22) |
| | 12 | 0.84(0.017) | 1.29(0.24) | 0.99(0.18) |
| 283 | 14 | 0.87(0.017) | 1.08(0.15) | 0.89(0.12) |
| | 16 | 0.88(0.011) | 0.84(0.12) | 0.66(0.09) |
| | 18 | 0.92(0.013) | 0.88(0.15) | 0.48(0.08) |
| | 20 | 0.95(0.012) | 0.94(0.15) | 0.42(0.07) |
| | 10 | 0.41(0.019) | 4.40(0.88) | 6.20(1.24) |
| | 12 | 0.47(0.016) | 4.69(0.69) | 4.94(0.73) |
| 293 | 14 | 0.34(0.017) | 4.55(1.11) | 3.71(0.91) |
| | 16 | 0.38(0.013) | 4.72(0.77) | 3.93(0.64) |
| | 18 | 0.46(0.017) | 3.42(0.65) | 3.54(0.67) |
| | 20 | 0.55(0.020) | 3.65(0.72) | 2.85(0.56) |
| | 14 | 0.10(0.004) | 5.91(0.92) | 7.12(1.11) |
| | 17 | 0.14(0.005) | 7.77(1.00) | 6.43(0.83) |
| 303 | 20 | 0.21(0.004) | 5.56(0.46) | 6.25(0.52) |
| | 23 | 0.28(0.004) | 6.89(0.34) | 6.21(0.31) |

[a]Quasielastic cross section is assumed to be Rutherford.

states $q=18$, 19, and 20. The absolute values of the differential cross sections can be obtained from the cross-section ratios given in Table I.

Among the many versions of semiclassical theory in the literature,[2,3,7–9] that of von Oertzen *et al.*[3] is followed in this paper. Briefly, a quasielastic reaction occurs on the classically prescribed orbit with a probability $P$ that is particular to the reaction. Thus the differential cross section for a particular channel $i$ is

$$(d\sigma)_i = P_i(d\sigma)_{qe} = P_i(1-p_a)(d\sigma)_{sc} , \qquad (1)$$

where $\sum_i P_i = 1$, $(d\sigma)_{qe}$ and $(d\sigma)_{sc}$ are quasielastic and theoretical (e.g., Rutherford) scattering cross sections, and $p_a$ is the absorption probability into such nonquasielastic channels as fusion, deep inelastic, etc. The absorption in semiclassical theory is given by the mean-free-path attenuation of incident flux.[8] Experimentally, the quasielastic cross section $(d\sigma)_{qe}$ is obtained by adding contributions from all observed channels, and the ratio of transfer to the quasielastic cross section $(d\sigma)_i/(d\sigma)_{qe}$ is the transfer probability $P_i$. This probability can be factored as $P=tSF$ for one-nucleon transfer reactions. Here $t$ is the intrinsic probability (e.g., transmission coefficient in the tunneling model), $S$ accounts for nuclear structure (spectroscopic factors), and $F$ is a reduction factor to account for the orbit mismatch or perturbation (caused by $Q$ value, changes in $Z$, $M$, angular momentum, etc.). Von Oertzen *et al.*[3] give a detailed discussion of these factors, including comparisons of $F$ factors obtained by the semiclassical versus distorted-wave Born approximation (DWBA) method. The value of the probability for the whole orbit can be approximated by its value $t(D)$ at the perihelion, where the nuclei are separated by the apsidal distance $D$, and with this approximation the transfer probability becomes

$$P_i[D(E,\theta)] = Ct_i(D) , \qquad (2)$$

where $C$ stands for the product $SF$. An implicit dependence of $D$ on orbit parameters $E$ and $\theta$ is shown. The factor $C$ generally depends on collision dynamics as well as on nuclear structures;[1,3,4] however, previous studies[3–5] have shown that for cases such as this, where many individual transitions are included in the energy-integrated cross section, it is insensitive to, or even independent of, $E$ and $\theta$.

We first studied the shape of the measured transfer probability versus Coulomb apsidal distance $D_c$. For this purpose the ratios of transfer to quasielastic differential cross sections measured at four different energies were combined into common plots using the relation for Coulomb orbits

$$D_c = [(Z_p Z_t e^2)/(2E)(1+\csc)(\theta/2)] .$$

The results are shown in Fig. 2. If the short-range attractive nuclear force could be ignored, the probability should follow a straight line on a semilog plot; i.e.,

$$P(D_c) \propto \exp(-2kD_c) ,$$

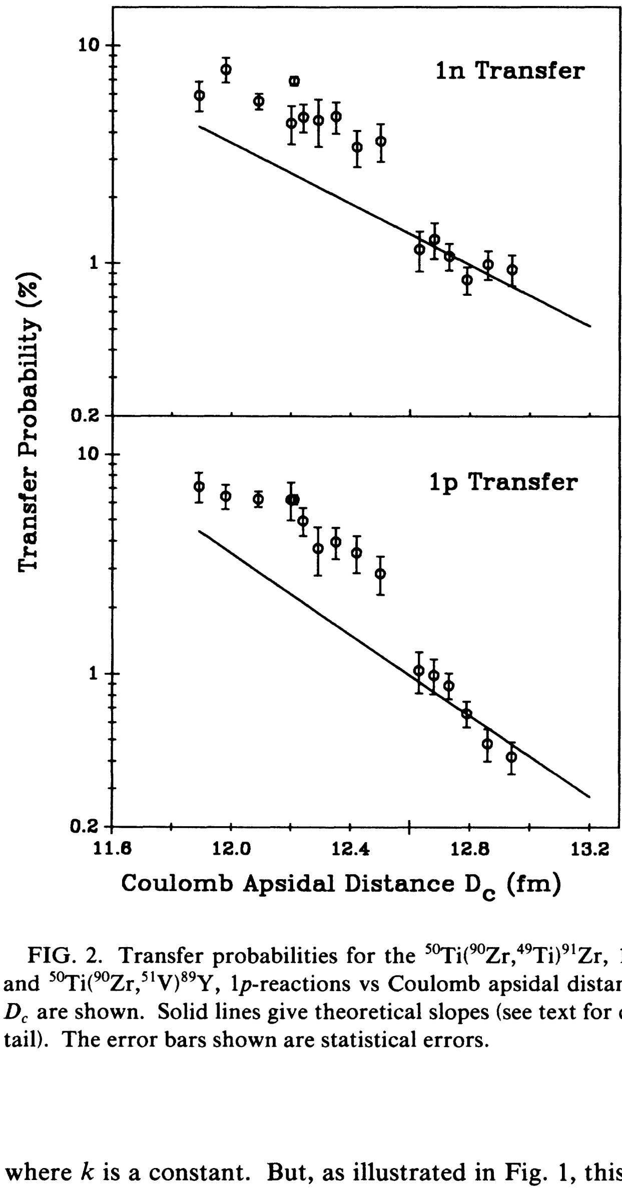


FIG. 2. Transfer probabilities for the $^{50}$Ti($^{90}$Zr,$^{49}$Ti)$^{91}$Zr, 1*n*- and $^{50}$Ti($^{90}$Zr,$^{51}$V)$^{89}$Y, 1*p*-reactions vs Coulomb apsidal distance $D_c$ are shown. Solid lines give theoretical slopes (see text for detail). The error bars shown are statistical errors.

where $k$ is a constant. But, as illustrated in Fig. 1, this is not the case. The slopes of the solid lines (shown in Fig. 2), which were drawn to represent large $D_c$ results, were calculated in the manner described herein. As has been pointed out by Körner *et al.*[10] and by Christensen *et al.*,[1] the deviation of the kind seen in Fig. 2 can result from the distortion of Coulomb orbits by the tail of the nuclear potential. The potential tail causes $P$ to rise faster by pulling the Coulomb orbit inward, forcing the actual apsidal distance to be smaller than the corresponding $D_c$. The rise ceases when the strong-absorption regime is reached, and the probability turns over, producing a shape similar to those seen in Fig. 2.

To find a realistic relation between the actual apsidal distance $D$ and angle $\theta$, a nucleus-nucleus potential was added to the deflection field, and then the orbit integral

$$\theta=\pi-2L(E,D)\int_D^{\infty}(E-U_N-U_c-U_L)^{1/2}\left[\frac{dr}{r^2}\right] \qquad (3)$$

was numerically evaluated. In this integral $L(E,D)$ is the classical angular momentum and $U_N$, $U_c$, and $U_L$ are the nucleus-nucleus, Coulomb, and centrifugal potentials, respectively. A Woods-Saxon equivalent of Lozano and Madurga's,[11] exponential potential, which represents the tail region especially well, was adopted for this calculation. The upper panel of Fig. 3 shows the combined height of $U_c$ and $U_N$ in the tail region. The top of the interaction $(U_c+U_N)$ barrier, which is reached at 11.30 fm, is 105.6 MeV. The lower panel shows $\theta$ vs $D$ at c.m. energies corresponding to the four experimental bombarding energies. (Since $D$ is directly related to the impact parameter or $L$, this figure, in effect, gives the classical deflection functions.) Also included in the same figure are the values of $D_c$ (solid curves) for reference. As expected, the added attractive potential does reduce apsidal distances. The orbits are so modified that the relation between $\theta$ and $D$ is still unique for three lower energies, but not for the highest. The interaction barrier $(U_c+U_N)$ is exceeded at the highest energy, and the relation is multivalued (in the angular range shown) because the paths of severely refracted (pulled inward) trajectories, which turn around at inner turning points, can merge with the

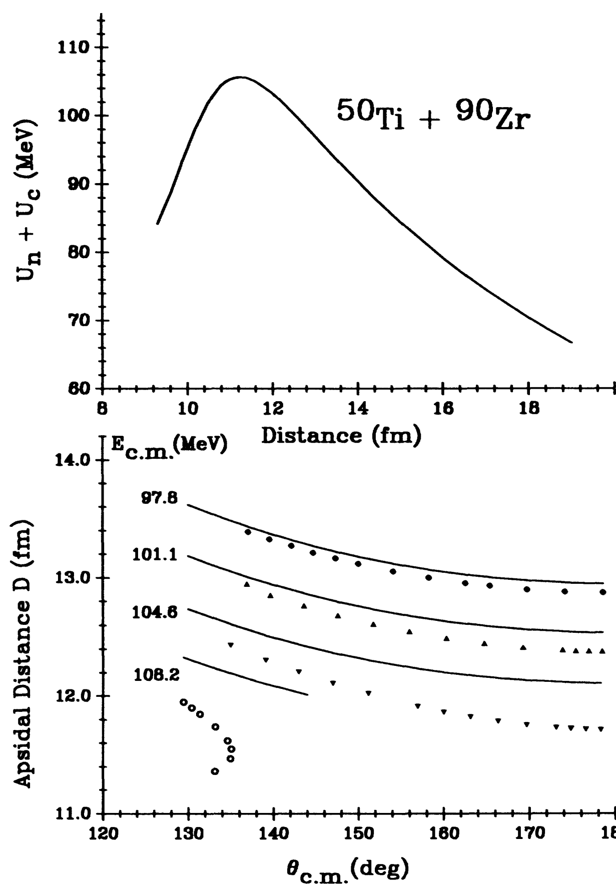


FIG. 3. The strength of the interaction potential $U_c+U_N$ used for the classical trajectory is shown as s function of internuclear separation distance in the upper panel. Apsidal distances calculated using the $U_c+U_N$ potential are shown by discrete points for the four energies and backward angles in the lower panel. The solid curves of the lower panel give Coulomb $(U_N=0)$ results.

paths followed by more distant trajectories, which turn around at outer turning points. (See, for example, Ref. 8 for these and more complicated trajectories.) Small changes of the values of diffuseness or strength parameters of the nucleus-nucleus potential do not alter the $\theta$ vs $D$ relation significantly.

The measured probabilities replotted versus new apsidal distance are presented in Fig. 4. Although the theory is not applicable, the cross-section ratios of those close collisions for which the outer turning points do not exist are included in the figure for sake of completeness. They are shown in the hatched areas. The solid curves are predictions of transfer probabilities form the tunneling model of Brosa and Gross.[12] In this model the nucleon-transfer probability is given in terms of the probability of a valence nucleon, which is initially bound in the potential well of the core nucleus, to be found in the potential well of the other nucleus by tunneling through the barrier that is created by the overlapping tails of the two potential wells (i.e., nucleon transmission coefficient is the intrinsic probability). The tunneling transmission coefficient $t(D)$ was calculated by both the parabolic- and

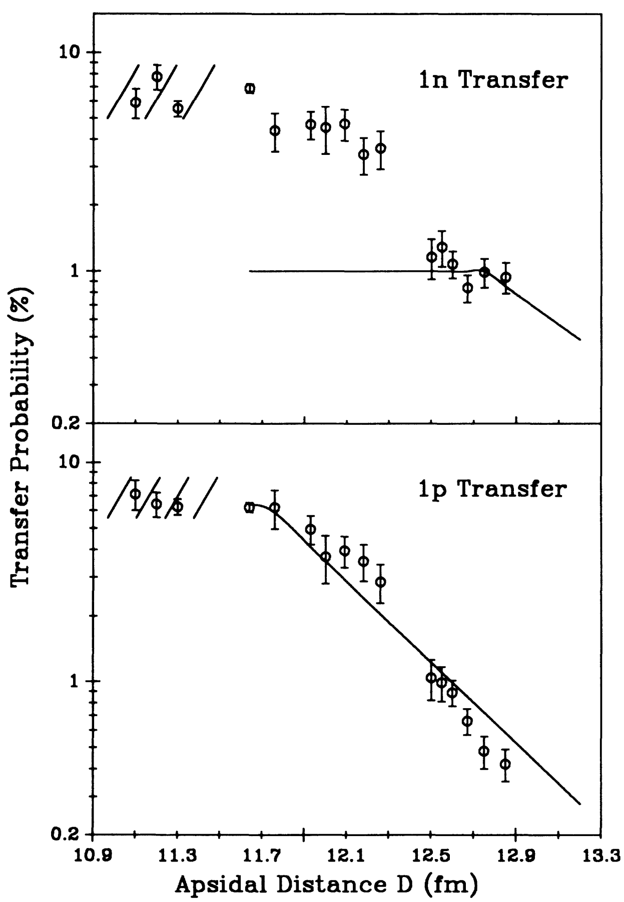


FIG. 4. Experimental transfer probabilities plotted versus apsidal distance $D$ (shown on Fig. 3) are compared to the tunneling model predictions (solid lines). See text for the explanation of the hatched areas. The error bars shown are statistical errors.

WKB-approximation methods. The well shape was assumed frozen during the collision. The standard[13] nucleon-nucleus potentials and the known nucleon binding energies, $B_n = 10.9$ and $B_p = 8.4$ MeV, were used. Both methods gave results that are practically identical: $t(D)$ is of $\exp[k(D_0 - D)]$ form, where $k$ and $D_0$ are constants. This is the form expected from the DWBA (Ref. 7) and other theories[9,14] at large internuclear distances. The value of $k$ for the neutron transfer is primarily determined by the binding energy, whereas the $k$ value for the proton transfer is determined by the binding plus Coulomb repulsion energy (the proton $k$ value is about 30% larger than the neutron $k$ value although the binding energy is substantially less). Because of the Coulomb repulsion, the value of $D_0$ for the proton is smaller (by about 1 fm) than the neutron value. For a given binding energy (neutron) or binding plus Coulomb energy (proton), the well radii, i.e., $r_0 A_p^{1/3}$ and $r_0 A_T^{1/3}$, are the critical factors determining the value of $D_0$. Diffuseness and depth of the nucleon-nucleus potential wells influence these constants only mildly. The nucleon transmission coefficient $t(D)$ rises linearly on a semilog plot as the barrier becomes lower with decreasing $D$, but saturates once the barrier height becomes equal to or lower than the binding energy (i.e., $t(D) = 1$ for $D \leq D_0$). This feature of the model is illustrated by the theoretical results (solid lines) shown in Fig. 4, after scaling to represent the data. The theory reproduces the observed $1p$-transfer feature very well, including the saturation at correct $D$. The same theory, on the other hand, gives much smaller $1n$-transfer probability. This follows because the theory predicts an early onset of the saturation. A substantial (0.3 fm or more) shift of this onset can be obtained if a correspondingly large change of the well radii

$$(\Delta D_0 / D_0 = \Delta r_0 / r_0)$$

is made. But such a change results in "wrong" nucleon wells and hence is not a viable procedure. Reasonable changes ($\pm 5\%$) of the value of the diffuseness or depth do not yield comparable shifts of $D_0$.

The saturation of the transfer probability is based on the one-dimensional tunneling model, in which the transfer probability is assumed to be the transmission coefficient of the barrier at the saddle point. This is a reasonable assumption for distant collisions since the contribution away from the saddle point is insignificant due to the rapidly increasing barrier, but needs closer scrutiny for $D \simeq D_0$ and smaller. For example, if the nucleon gets excited prior to transfer, or if the tunneling becomes multidimensional[15] inside $D_0$, or if equivalently a neck[16,17] is formed, then the neutron-transfer probability continues to increase through this newly acquired mechanism. Whatever its nature, Fig. 4 shows that the mechanism affects the neutron transfer but not the proton transfer.

Stelson[18] found the principal coupling mechanism that enhances fusion of heavy nuclei at subbarrier energies to be the free flow of a neutron between the interacting nuclei. (The free flow commences when the barrier tunneling probability becomes 100% [i.e., $t(D) = 1$].) Stelson established a systematic correlation between $D_0$ and fusion "threshold" from the analysis of an extensive body of fusion cross-section data. The head-on collision apsidal distance, $D(\theta=180°)$, corresponding to the fusion threshold (100.9 MeV) for the present system, which was determined from the experimental data,[19] is 12.38 fm. This value is very close to $D \sim 12.5$ fm where the $1n$-transfer data begin to deviate from the tunneling theory prediction. The similarity of these distances suggests that the free flow of a neutron is responsible for the large neutron-transfer probability, as well as the enhanced fusion cross section. This mechanism contrasts with that which was considered in Ref. 20 where the enhancement of the fusion cross section is obtained at the expense of the neutron-transfer cross section. Since the neutron free flow takes place at relatively large internuclear distances, and since the exchange force arising from it (neutron free flow) can provide additional attraction that hastens the amalgamation of the collision partners, it is very tempting to associate the neutron free flow with the initial stage of the neck formation.[16,17] If this association is valid, the neck enhances the neutron-transfer cross section as well as the fusion cross section.

This investigation is being extended to include similar studies of neighboring systems with the hope of gaining a firmer understanding of quasielastic reactions near the barrier, especially between medium mass nuclei.

We acknowledge useful discussion with M. L. Halbert. This research was supported by the Office of Basic Energy Sciences, U. S. Department of Energy, under Contract No. DE-AC05-84OR21400 with Martin Marietta Energy Systems, Inc.

[1]P. R. Christensen *et al.*, Nucl. Phys. **A207**, 33 (1973).
[2]K. Alder *et al.*, Nucl. Phys. **A191**, 399 (1972).
[3]W. von Oertzen *et al.*, Z. Phys. A **326**, 463 (1987).
[4]H. Siekmann *et al.*, Z. Phys. A **307**, 113 (1982).
[5]G. Wirth *et al.*, Phys. Lett. B **177**, 282 (1986); G. Himmele *et al.*, Nucl. Phys. **A404**, 401 (1983).
[6]D. Shapira *et al.*, Nucl. Instrum. Methods **169**, 77 (1980).
[7]L. J. B. Goldfarb and W. von Oertzen, in *Heavy Ion Collisions,* edited by R. Bock (North-Holland, Amsterdam, 1979), Vol. 1, Chap. 2.
[8]R. A. Broglia and A. Winther, *Heavy Ion Reactions Lecture Notes* (Benjamin/Cummings, Reading, MA, 1981), Vol. 1, Chap. 3.
[9]W. Norenberg and H. A. Weidenmuller, in *Introduction to the Theory of Heavy-Ion Collisions,* Vol. 51 of *Lecture Notes in Physics,* edited by J. Ehlers, K. Hepp, H. A. Weidemuller, and J. Zittartz (Springer-Verlag, Berlin, 1976).
[10]H. J. Korner *et al.*, Phys. Rev. C **7**, 107 (1973).
[11]M. Lozano and G. Madurga, Nucl. Phys. **A334**, 349 (1980).
[12]U. Brosa and D. H. E. Gross, Z. Phys. A **298**, 91 (1980).
[13]A. Bohr and B. R. Mottelson, *Nuclear Structure* (Benjamin, New York, 1969), Vol. 1, p. 236ff.
[14]A. Trabert, D. Trautmann, and K. Alder, Z. Phys. A **281**, 391 (1977).
[15]H. J. Krappe *et al.*, Z. Phys. A **314**, 23 (1983).
[16]C. E. Aguiar *et al.*, Nucl. Phys. A **472**, 571 (1987).
[17]A. Iwamoto and K. Harada, Z. Phys. A **326**, 201 (1987).
[18]P. H. Stelson, Phys. Lett. B **205**, 190 (1988).
[19]P. H. Stelson *et al.*, Oak Ridge National Laboratory Report No. ORNL-6233, 1986.
[20]R. Broglia *et al.*, Phys. Rev. C **27**, 2433 (1983).